Anticipative Control of Low-Power Wind Energy Conversion Systems for Optimal Power Regime

C. Vlad, I. Munteanu, A.I. Bratcu, E. Ceangă

Dunărea de Jos University of Galaţi, 47, Domnească, 800008-Galaţi
Romania (Tel: 0040-236-470-905; e-mail: ciprian.vlad@ugal.ro; iulian.munteanu@ugal.ro, antoneta.bratcu@ugal.ro, emil.ceangă@ugal.ro)

Abstract: In this paper a novel anticipative control structure for WECS (Wind Energy Conversion System) operating at MPP (Maximum Power Point), which allows the improvement of the rotational speed closed-loop dynamics, is presented. The main idea is based on the remark that the wind speed acts upon the controlled plant as a disturbance and simultaneously generates the set point of the MPP control loop. An extensive comparative analysis of this new control structure is made with respect to the classical LQ control approach. The superiority of this new approach, consisting in better energy efficiency obtained with less control input effort, is illustrated for a permanent-magnet-synchronous-generator (PMSG)-based WECS by numerical simulation. The proposed control structure has been experimentally validated by using a real-time wind turbine electromechanical simulator.

Keywords: Windmills, Maximum power point tracking, Linear quadratic control, Feedforward control, System identification, Permanent magnet synchronous motors.

1. INTRODUCTION

The automatic control of wind energy conversion systems (WECS) is one of the main problems in the renewable energy conversion field. Most of the control problems are caused by the fact that the wind speed is a non-stationary random process, with spatial distribution and possible extreme variations [Nichita, C. et al. (2002) and Diop, A.D. et al. (2007)]. Usually, the WECS control deals with a multi-criteria objective, with various components, such as wind turbine power limitation in full-load operating mode, the alleviation of the wind turbulence-generated mechanical fatigue, maximization of the captured energy in partial-load mode, the reduction of the torsion vibrations in the mechanical structure etc. [Bianchi, F. et al. (2006), Burton, T. et al. (2001), Camblong H. et al. (2006), Leithead, W.E. et al. (1991) and Munteanu, I. et al. (2008)]. The WECS control in order to ensure maximum power point tracking (MPPT) in partial-load operating mode is a problem of significant interest, as considered in Camblong H. et al. (2006), Munteanu, I. et al. (2008), , Senjiyu, T. et al. (2006), Tan K. and Islam S. (2004)].

An important design solution in WECS technology is to use the multi-polar PMSGs. The PMSG-based solution is widely used in low-power wind systems, especially when operating in isolated site, as it allows the direct coupling between the generator and the wind shaft.

There are various control solutions depending on the load nature, as proposed in Arifujjaman, Md. et al. (2008), Borowy, B. and Salameh, Z.M. (1997), Cutululis, N.A. et al. (2006), De Broe, A.M. et al. (1999) and Martinez, J. et al. (2006). Regarding the WECS-related control methodologies, beside the classical (widely used) control algorithms, various and more complex techniques such as the feedback linearization control [Cutululis, N. A. (2004)] or robust control (QFT and multi-model techniques) [Cutululis, N.A. et al. (2006)] are proposed in the literature. This continuous research is due mainly to the nonlinear and variant nature of the controlled plant and to the fact that it is subjected to erratic wind speed variations. Also, significant difficulties are encountered when testing these algorithms in deterministic conditions. That's why, in most of the technical articles, the proposed solutions are supported by results provided by numerical simulation.

In this paper the optimal wind energy conversion mode based on the shaft rotational speed control structure is analyzed. The paper highlights the specific aspects of this problem, obtained through experimental tests, and proposes an appropriate anticipative solution to meet the efficiency and simplicity specifications. This solution was validated using an experimental test rig, which is briefly presented in the paper. To underline the superiority of this new method, an extensive comparative analysis of this new control structure is made with respect to the classical LQ control approach.

The paper is structured as follows: section 2 presents the basic wind conversion system modelling and the MPPT control principles and structures provided by the literature. In the next section, the third, the LQ and the anticipative control laws synthesis are presented. Section 4 presents the experimental test rig, the results concerning the wind conversion system identification and the experimental validation of the proposed control solution. Comparative simulation results are showing the anticipative structure superior behaviour with respect to the classical LQ control law. Finally, the paper ends with the conclusions regarding the obtained experimental results.

2. MODELLING AND CONTROL SYSTEM ANALYSIS

2.1 Problem statement

Figure 1 shows the structure of the low-power wind energy conversion system connected to an insulated local grid, as considered in this paper. The PMSG is directly connected to the rotor turbine shaft. It feeds a DC-link through a diode rectifier and a chopper. The inverter feeds the AC local grid with acceptable values of voltage and frequency. The wind power system load can be adjusted by the chopper output and the exceeding energy is injected into the accumulator battery.

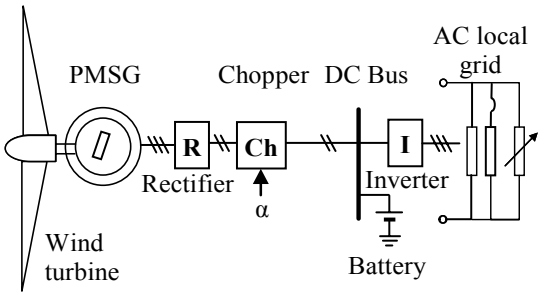

Fig. 1. Autonomous wind power system structure

In the partial-load mode, the chopper control input must ensure the optimal wind energy conversion for various values of wind speed and/or the local grid load.

2.2 Wind turbine model

The average mechanical power developed by a wind turbine, P_m is:

$$P_m = 0.5\pi\rho A w^3 C_p \tag{1}$$

where ρ - is the air density; A – rotor swept area, w – single point wind speed in the rotor axial direction and C_p - is the power coefficient. Wind energy conversion efficiency is determined by the power coefficient value, which depends on the tip speed ratio of the wind turbine, λ. The tip speed ratio is defined as the ratio between the peripheral speed of the blades and the wind speed: $\lambda = R\Omega/w$, where R is the blade length. Relation (1) is more known in the form below,

$$P_m = 0.5\pi\rho w^3 R^2 C_P(\lambda) \tag{2}$$

and the wind torque is:

$$T_w = P_m / \Omega = 0.5\pi\rho w^2 R^3 C_T(\lambda) \tag{3}$$

where $C_T(\lambda)=C_p(\lambda)/\lambda$ is called the torque coefficient.

In Figure 2 are presented the power $P_m(\Omega,w)$ and the torque $T_w(\Omega,w)$ characteristics of the low power wind turbine investigated in this work.

The $C_p(\lambda)$ characteristic [Munteanu, I. et al. (2008)] has a maximum for a well-determined tip speed, λ_{opt}, corresponding to optimum operating regime in relation to the energy efficiency criterion.

In $P_m(\Omega,w)$ - Ω plane, this regime corresponds to the locus formed by the $P_m(\Omega,w)$ characteristics maxima, named the optimal regimes characteristic, ORC (see Figure 2).

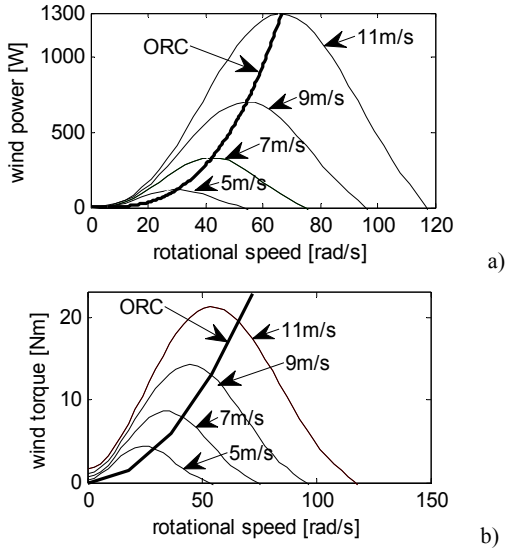

Fig. 2. The optimal regime characteristics in the: a) $P_m - \Omega$ plane; b) $T_W - \Omega$ plane

For the considered wind turbine, the torque coefficient characteristic can be modelled as:

$$C_T(\lambda) = \sum_{i=0}^{6} a_i \lambda^i \tag{4}$$

where the a_i, $i = \overline{0,6}$ parameters were determined by polynomial regression, from the mechanical turbine characteristic (see Appendix A).

2.3 PMSG model

For wind turbine systems in island operation, the PMSG should be considered as a multivariable system with 3 inputs: active shaft torque developed by the wind turbine, T_w, load resistance, R_l, load inductance, L_l, and 3 outputs: i_d, i_q currents (possibly u_d, u_q voltages) and shaft rotational speed Ω. The equivalent load of the generator is changed by the chopper's output (see Figure 1).

The PMSG model used in this paper is in (*d,q*) frame [Leonhard, W. (2001)]. The mathematical model of the PMSG directly connected to the turbine shaft [Cutululis, N.A. and Ceangă, E. (2004)] is:

$$\begin{cases} (L_d + L_l)\dfrac{\mathrm{d}i_d}{\mathrm{d}t} = -(R_S + R_l) i_d + p(L_q - L_l) i_q \Omega_r \\ (L_q + L_l)\dfrac{\mathrm{d}i_q}{\mathrm{d}t} = -(R_S + R_l) i_q - p(L_d - L_l) i_d \Omega_r + p\Phi_m \Omega_r \\ J\dfrac{\mathrm{d}\Omega_r}{\mathrm{d}t} = T_w - p\left[(L_d - L_q) i_d i_q - \Phi_m i_q\right] \end{cases} \tag{5}$$

where the electromagnetic torque is obtained as:

$$T_{em} = p\left[\Phi_m i_q - \left(L_d - L_q\right) i_d i_q\right] \tag{6}$$

In (5) and (6) the notations are as follows. p is the number of pole pairs, Φ_m is the flux linkage, L_d, L_q are d and q inductances, R_s is the stator resistance, J is the rotor shaft moment of inertia, Ω is the shaft rotational speed and T_w is the active shaft torque developed by the wind turbine.

2.4 State-space model for the wind power system

The dynamic of the power electronics was neglected because is significantly faster than that of the wind turbine. In addition, the PMSG equivalent load is considered resistive (L_l=0). The plant has two exogenous variables: wind speed w and the equivalent load resistance at generator terminals, R_l, modified by the chopper operation. Replacing in (5) the wind torque expression from (3) and defining the state and input vectors as

$$\begin{bmatrix} x_1(t) \\ x_2(t) \\ x_3(t) \end{bmatrix} = \begin{bmatrix} i_d(t) \\ i_q(t) \\ \Omega(t) \end{bmatrix}; \begin{bmatrix} u_1(t) \\ u_2(t) \end{bmatrix} = \begin{bmatrix} v(t) \\ R_l(t) \end{bmatrix} \tag{7}$$

the state model of PMSG operating on an insulated load becomes:

$$\frac{\mathrm{d}}{\mathrm{dt}}\begin{bmatrix} x_1 \\ x_2 \\ x_3 \end{bmatrix} = \begin{bmatrix} \frac{1}{L_d}\left(-R_S x_1 + pL_q x_2 x_3\right) \\ \frac{1}{L_q}\left(-R_S x_2 - pL_d x_1 x_3 + p\Phi_m x_3\right) \\ -\frac{1}{J} p\left[\Phi_m x_2 - \left(L_d - L_q\right) x_1 x_2\right] \end{bmatrix} + \tag{8}$$

$$+\begin{bmatrix} -(1/L_d)x_1 \\ -(1/L_q)x_2 \\ 0 \end{bmatrix} \cdot R_l + \begin{bmatrix} 0 \\ 0 \\ 1/J \end{bmatrix} \cdot 0.5\pi\rho w^2 R^3 . C_T\left(Rx_3 / w\right)$$

2.5 WECS control outline

The optimal energy conversion of the fixed-pitch wind turbine operating in partial-load mode is performed by means of the chopper control input. When λ_{opt} and $C_{p_{\max}} = C_p\left(\lambda_{opt}\right)$ are known, in order to maintain the operating point to the ORC, three main control solutions are provided in the literature [Munteanu, I. et al. (2008)]:

I. *Shaft rotational speed control* (as shown in Figure 3). The reference of the speed loop is based on the wind speed measurement:

$$\Omega_{opt}(t) = (\lambda_{opt} / R) \cdot w(t) \tag{9}$$

II. *Wind torque control to its optimal value*. The set point depends on the shaft rotational speed value:

$$T_{w_{opt}} = T_w^{ref} = K \cdot \Omega^2 \tag{10}$$

K is given by:

$$K = \frac{1}{2}\rho\pi \frac{C_p(\lambda_{opt})}{\lambda_{opt}^3} R^5 \tag{11}$$

III. *Power control to its optimal value* dependent on the shaft rotational speed. The power reference is:

$$P_{opt} = P^{ref} = K \cdot \Omega^3 \tag{12}$$

where K is given by (11).

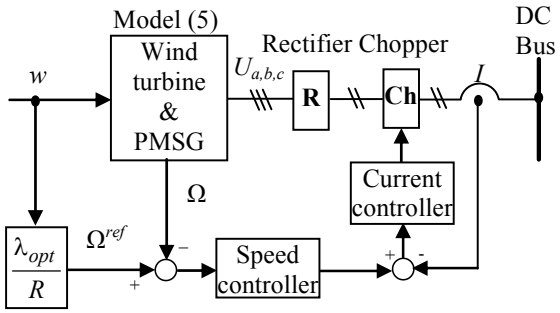

Fig. 3. Rotational speed control loop

In the following the paper discourse is focused on the rotor shaft rotational speed control structure. In this context, two control law solutions are separately synthesized and compared.

3. CONTROL LAWS SYNTHESIS

3.1 The control loop features

In general, on a classical control loop – as is the case of the WECS power control structure in the full-load zone – there are acting two independent exogenous: the reference and the disturbance. In the optimal speed control value structure (see Figure 3 and Figure 4), there is only one exogenous input, namely the wind speed. This generates the reference through a fast feed-forward connection (without dynamics), and represent, in the same time, the plant disturbance variable.

A physical analysis of the control system highlights some important features. Supposing that the exogenous variable (the wind speed) changes for example with a positive step, then the feed-forward link imposes an increase of the rotational speed reference and the controller will drive the PMSG towards higher speeds (unloading action). Meanwhile, the direct effect of exogenous input variation is the wind torque increase, so, the shaft rotational speed will also increase (assuming that the wind power system load remains constant). These two actions on the process, coming from the same source, have effects in the same direction and cause a significant rotational speed overshot, which is at least annoying. It is desirable that the loop tuning methodology

takes into account this feature of the rotational speed control structure when the system operates on ORC.

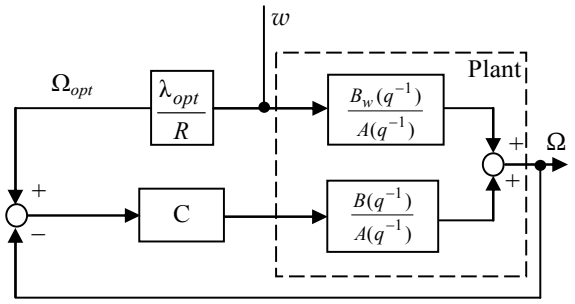

Fig. 4. Rotational speed optimal control structure

Two solutions of control law synthesis for the mentioned speed loop are analyzed in the following. The first is related to an optimal LQ control approach developed on the classical structure from Figure 4. The second solution is based on an anticipative control structure justified by the above-described feature. In the next section, the performances of these approaches are comparatively analyzed by numerical simulation and then, the selected solution is experimentally validated by using a real-time wind turbine electromechanical simulator.

3.2 LQ optimal control

In general, the WECS control problem embeds a multi-criterion objective. Beside the energy maximization by controlling the rotational speed at the optimal value, additional requirements are also imposed, such as alleviating the mechanical structure fatigue loads and/or increasing the battery life. The shaft rotational speed efficient control, based upon the energy criterion is realized by varying the chopper control input and induces high-frequency high-amplitude electromagnetic torque variations. These have antagonistic effects concerning the requirements imposed by the additional listed criteria. Strong torque variations generate fatigue stress and at the same time, induce significant current variations in the battery charging circuit (see Figure 1), which reduces its life. The trade-off between two opposed requirements can be achieved by a LQ control. It uses a mixed performance criterion, *J*, which includes square speed tracking error at the computing step (*i*+1) and square control output variations at step (i):

$$J=[y^{sp}(i+1)-y(i+1)]^2+\rho\cdot\Delta u^2(i) \tag{13}$$

$y(i)$ and $\Delta u(i)$ are the plant output and control input variations at the discrete time *i*. In the criterion (13) the reference is known based on the one-step prediction of the wind speed, while the output must be replaced with a prediction, $\hat{y}(i+1)$. To obtain this prediction, one starts from the plant discrete-time model, considered as

$$A(q^{-1})y(i)=B(q^{-1})u(i)+B_w(q^{-1})w(i) \tag{14}$$

where

$$A(q^{-1})=1+a_1q^{-1}+\ldots+a_nq^{-n}$$
$$B(q^{-1})=b_1q^{-1}+\ldots+b_mq^{-m}$$
$$B_w(q^{-1})=b_{w,1}q^{-1}+\ldots+b_{w,m_w}q^{-m_w}$$

If (14) is put in the form:

$$y(i)=q^{-1}A^*(q^{-1})y(i)+q^{-1}[q^{-1}B^*(q^{-1})+b_1]u(i)+,$$
$$+B_w^*(q^{-1})w(i-1) \tag{15}$$

in which

$$A^*(q^{-1})=-a_1-a_2q^{-1}-\ldots-a_nq^{-n+1}$$
$$B^*(q^{-1})=b_2+b_3q^{-1}+\ldots+b_mq^{-m+2}\ ,$$
$$B_w^*(q^{-1})=b_{w,1}+\ldots+b_{w,m_w}q^{-m_w+1}$$

one obtains:

$$y(i)=A^*\left(q^{-1}\right)y(i-1)+B^*\left(q^{-1}\right)u(i-2)+b_1u_1(i-1)+$$
$$+B_w^*(q^{-1})w(i-1) \tag{16}$$

Here, to obtain the model of system output prediction, $\hat{y}(i+1)$, the discrete time step is advanced by one. With this prediction, the criterion (13) becomes:

$$J=\left\{y^{sp}(i+1)-\left[1+(1-q^{-1})A^*(q^{-1})\right]y(i)-b_1\Delta u(i)\right.$$
$$\left.-B^*(q^{-1})\Delta u(i-1)+B_w^*(q^{-1})\Delta w(i)\right\}^2+\rho\Delta u^2(i), \tag{17}$$

and the optimal control input variation is:

$$\Delta u(i)=\eta\{y^{sp}(i+1)-[1+(1-q^{-1})A^*(q^{-1})]y(i)-$$
$$-B^*(q^{-1})u(i-1)-B_w^*(q^{-1})\Delta w(i)\}, \tag{18}$$

where $\eta=b_1/(b_1^2+\rho)$

The LQ optimal control structure of the shaft rotational speed is shown in Figure 5.

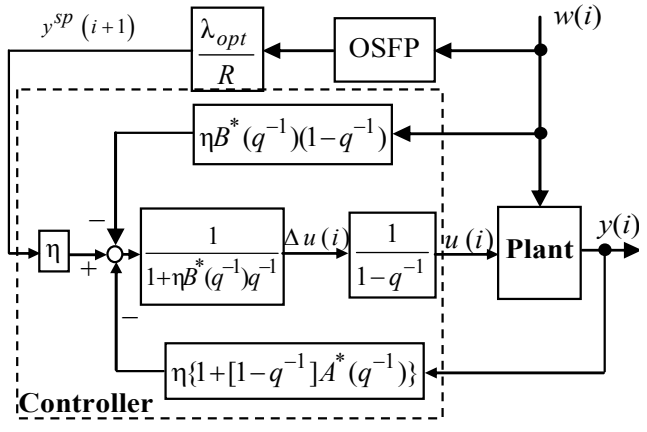

Fig. 5. LQ optimal control scheme

The OSFP (One Step Forward Predictor) block is used to advance the discrete time step in order to obtain the reference prediction.

3.3 Anticipative control solution

Unlike the above-presented LQ control law, in the following it is synthesized a composite control law, which includes two components:

- an anticipative component, u_a, depending on wind speed w:

$$u_a(i) = H_a(q^{-1})w(i) \tag{19}$$

where $H_a(q^{-1})$ is a causal limit approximation of $B_w(q^{-1}) / B(q^{-1})$;

- a feedback component, u_{fb}, computed according to the pole-placement method. Assuming that $B(z)$ is a monomial or a polynomial which does not introduce oscillating modes (hypothesis verified in practice - see next section), the discrete transfer function of the closed-loop system is:

$$H_0(z) = K\frac{z^{-1}}{(1-z_a z^{-1})(1-z_b z^{-1})} \tag{20}$$

where z_a and z_b poles are calculated so that the system has the required overshot, s (typically, s=4,3%) and the response time, t_r. Further, the second-order system parameters are calculated as in Ceangă, E. et al. (2001):

$$\varsigma = -\ln s / \sqrt{\pi^2 + (\ln s)^2}\ ;$$
$$\omega_n = -\ln\left(0.05\sqrt{1-\varsigma^2}\right) / (\varsigma t_r) \tag{21}$$

and then the assigned poles are obtained as

$$z_{a,b} = \rho.\mathrm{e}^{\pm j\theta} \tag{22}$$

where

$$\rho = \exp(-\varsigma\omega_n T_s);\quad \theta = \omega_n\sqrt{1-\varsigma^2}.T_s \tag{23}$$

Constant K from (20) results from imposing a zero steady-state error:

$$K = (1-z_a)(1-z_b) \tag{24}$$

The controller transfer function becomes

$$H_c(z) = \frac{A(z)}{B(z)}.\frac{Kz^{-1}}{(1-z_a z^{-1})(1-z_b z^{-1}) - Kz^{-1}} \tag{25}$$

The closed-loop system diagram representing the WECS anticipative rotational speed control is presented in Figure 6.

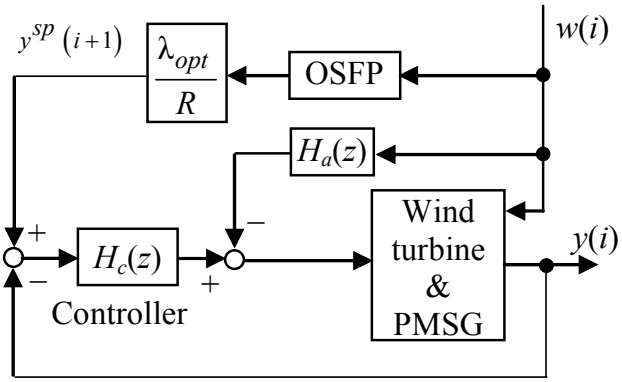

Fig. 6. The anticipative rotational speed control structure

4. EXPERIMENTAL RESULTS

4.1 Experimental test rig

The test rig was built as a development system that aims at experimentally researching the low-power hybrid renewable energy systems used for distributed production. It is composed of two subsystems: electromechanical wind turbine simulator and control/supervision subsystem.

The electromechanical wind turbine simulator (see Figure 7) is built based upon the hardware-in-the-loop simulation concept [Munteanu, I. et al. (2008)]. This simulator provides a "wind-powered like shaft" where the steady-state and dynamic characteristics of a given turbine can be replicated. The wind turbine shaft is directly coupled to a Southwest Windpower® Whisper WHI 200 PMSG, having 1 kW rated power.

An important function of the software application is the real-time wind speed generation. The subsystem achieving this function can ensure two distinct regimes:

a – constant wind speed regime, adjustable in real time through the ControlDesk® interface accompanying the dSPACE board;

b – turbulent wind regime, where the average wind speed is adjustable in real time through the ControlDesk® interface.

The experimental rig structure has a load adaptation circuit in order to ensure turbine operation on the ORC. The load adaptation circuit, coupled at the PMSG output, is composed of a rectifier and a chopper (see Figure 7).

The hardware and software support of the whole experimental rig is ensured by the dSPACE board DS 1103. The sampling time of the real-time application is 0.2 ms.

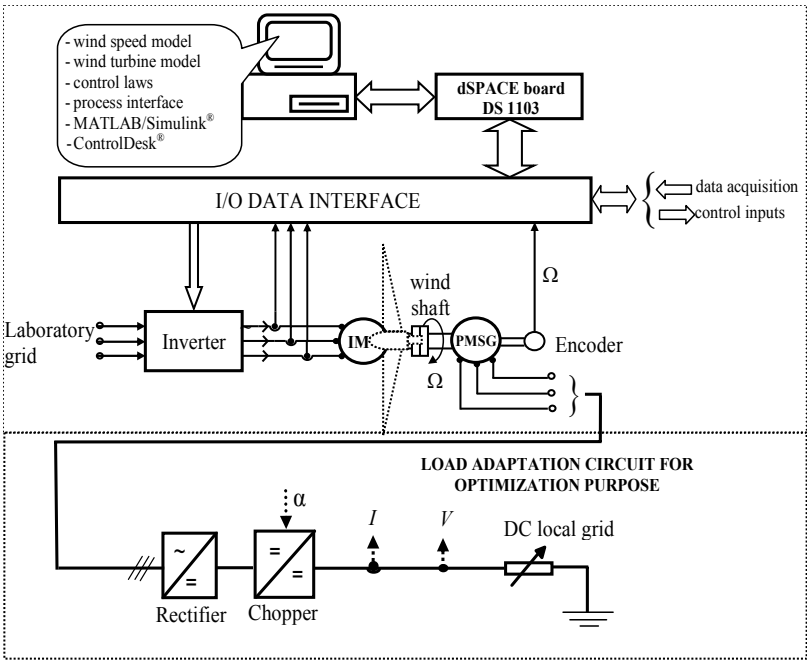

Fig. 7. Block diagram of the experimental rig

4.2 Experimental results obtained using a classical control structure

The first experimental tests were performed in order to establish the performance of the speed control loop based on the classical PI controller. The aim is to validate the conclusions of the analysis in section 3.1 regarding the presence of an important overshot. This is due to the fact that a wind speed variation yields initially two separate actions on the process (through reference and disturbance). The effects of these two separate actions cause rotational speed variations of the same sign.

In Figure 8, a screenshot of the experimental rig Control Desk® interface is given, illustrating the system response variation of loop reference generated by a wind speed step (see Figure 8a).

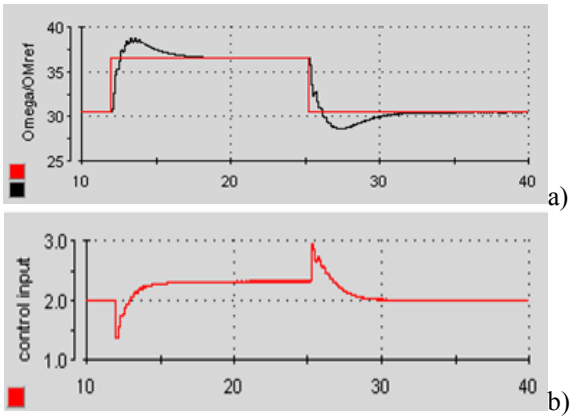

Fig. 8. Control Desk® screenshot: a) PI-controlled system response; b) control input evolution

The associated controller output evolution is given in the Figure 8b); one can remark that in the first moments the control input evolves in the opposite sense in relation to the steady-state value. So, the system has "non-minimum phase" behaviour in relation with the control input, which can be explained given the plant characteristic features.

The speed overshot is maintained for any set of controller parameters values and for steady-state operating points in the entire operating range. Correspondingly, the control input has rapid variations without contributing effectively to the control efficiency.

4.3 System identification

The process identification was made on the experimental bench in two stages. First, wind speed step variations have been applied on the open-loop system, while keeping the DC load constant. The transfer function for the wind speed – to – rotational speed channel (see Figure 4) was identified by using the instrumental variables method.

In the second phase the transfer function for the control input – to – rotational speed channel was identified. After eliminating the insignificant modal components, the identified model of the analyzed system is presented in Figure 9. The associated parameters are: $a_1 = 1.9956$, $a_2 = 0.9956$, $b_1 = -0.01932$, $b_2 = -0.01927$, $b_{w,1} = 0.02499$, $b_{w,2} = 0.029425$.

In Figure 10a) are shown the real plant and the identified system responses for wind speed step variations. In Figure 10b) are given the real and the identified system responses for control input step variations.

These results illustrate the accuracy of the identification.

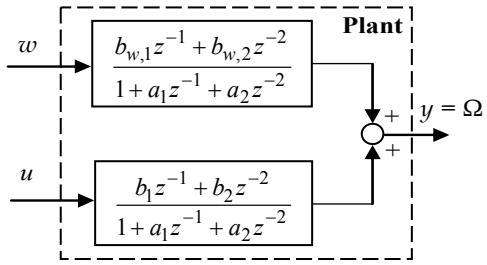

Fig. 9. The identified system structure

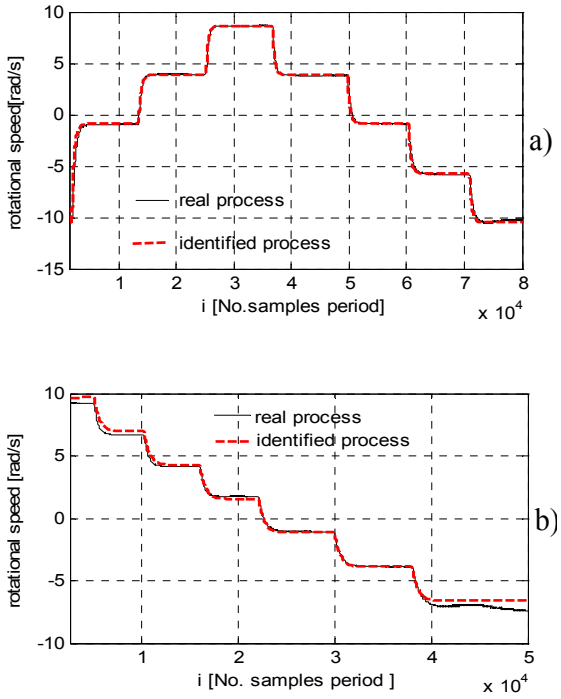

Fig. 10. Real plant and identified system response for: a) wind speed step variations; b) control input step variations

4.4 Preliminary validation of the control laws

Next, in order to perform a preliminary validation of the control structures presented in section 3 (Figure 5 and Figure 6), some numerical simulation results using the same mathematical model obtained by experimental identification, are analyzed. The objective is to compare the two control structures performances (in the exactly same conditions), in order to highlight the anticipative control structure superiority with respect to the classical ones (having in this case a LQ-computed controller).

In Figure 11 the performances of the "standard" control structure from Figure 5 while subjected to pseudo-random variations of wind speed, are presented. The first three evolutions (Figure 11a), b) and c)) correspond to a controller computed by solving the associated LQ problem using a weighting coefficient ρ = 0.5. One can observe the quite poor WECS energy efficiency shown by large deviations of the power coefficient under its maximal value (C_{pmax}=0.47), and large dispersion of the turbine operating point around the ORC. Correspondingly, the control effort is quite reduced (Figure 11b).

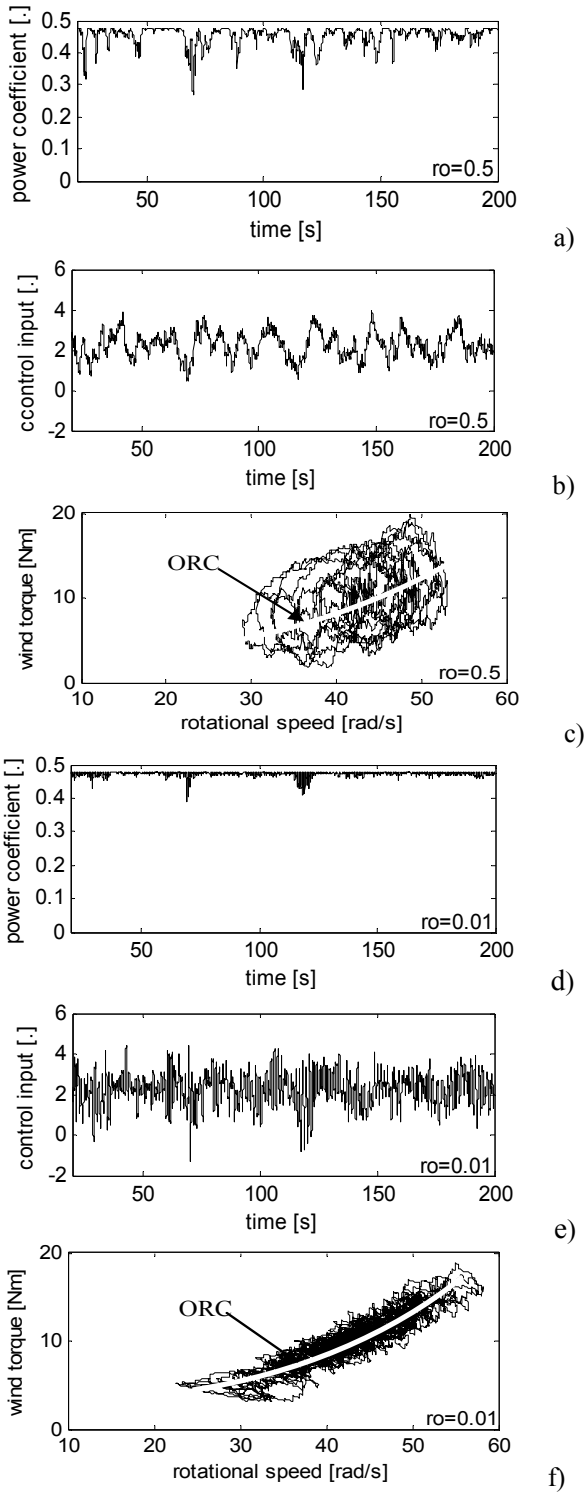

Fig. 11. LQ control results for ρ=0.5: a) power coefficient, b) control input, c) OP evolution around ORC; LQ control results for ρ=0.01: d) power coefficient, f) control input, f) OP evolution around ORC with the average wind speed about 7 m/s

The last three evolutions in Figure 11 (d), e) and f) show the controlled plant behaviour when the LQ controller parameters are computed using a much lower weighting coefficient value, $\rho = 0.01$.

The WECS presents high energy efficiency as the power coefficient is kept most of the time near to the optimum value and the operating point distribution around the ORC is reduced (see Figure 11f) comparatively with Figure 11c). But this energy performance is obtained with an important control effort (see Figure 11e) versus Figure 11b). These variations affect the mechanical structure by increasing the fatigue loads and reduce battery life as they induce significant variations of current in the battery circuit.

In short, the classical WECS speed control structure based on a LQ-computed controller provides versatility and means of obtaining higher energy efficiency by sacrificing system reliability.

Now, let us analyze the anticipative control structure from Figure 6 as the results in Figure 12 depicts. One can observe that the wind energy conversion performance is excellent, better than in the LQ case (ρ=0.01) (see Figure 12a) and c) versus Figure 11d) and f)). The very important result is that the control input variations are much lower (Figure 12b) with respect of any of the LQ cases (see Figure 12b) versus Figure 11b)). In short, the anticipative control law is far more powerful than the LQ control law, as it ensures better energy performance with less control effort. The transfer function of the anticipative computed controller is presented in Appendix B.

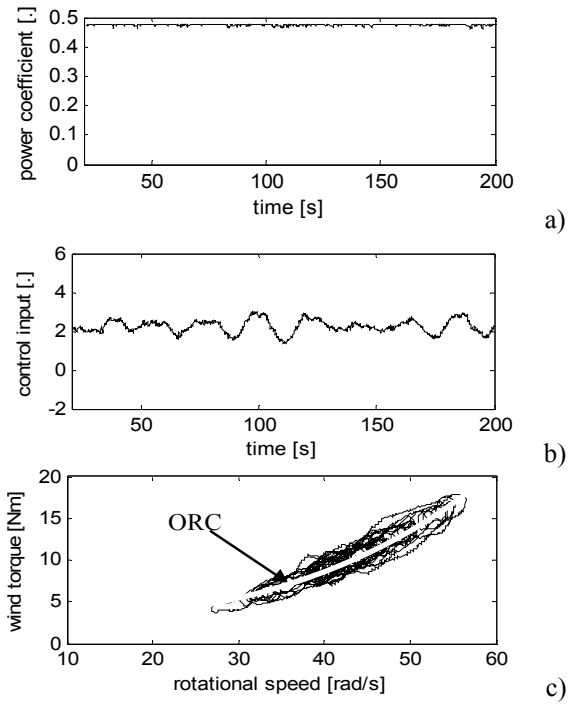

Fig. 12. WECS behaviour under anticipative control: a) power coefficient, b) control input, c) OP evolution around ORC with the average wind speed about 7 m/s

The conclusion that emerges from the analyzed control solutions is that the anticipative control structure is superior to the classical structures as it takes account the controlled plant feature presented in section 3.1. This structure has been implemented on the experimental test rig for more in-depth validations.

4.5 Experimental results obtained using the anticipative control structure

The first experimental test made with the anticipative control structure aimed at determining the system response to a step variation of the rotational speed setpoint, generated by wind speed variation (see relation (9)). In Figure 13 a screenshot from the ControlDesk® interface of the experimental test bench is given. By making a comparison with results in Figure 8, concerning the PI control classical structure, one can ascertain that the anticipative control structure has better dynamic performances.

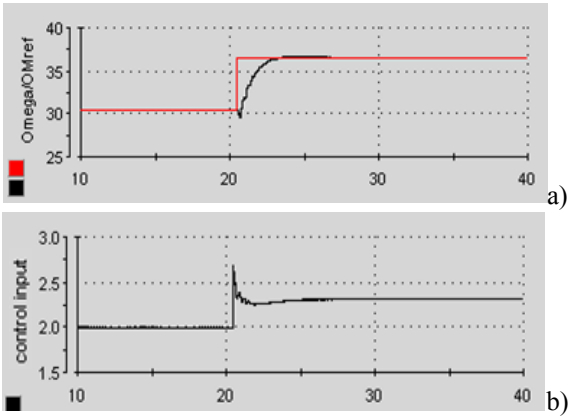

Fig. 13. Screenshot from ControlDesk® interface: a) system response with anticipative control structure; b) corresponding control input evolution

Secondly, experimental evaluation headed to validate the anticipative control while the WECS is subjected to pseudo-random variations of the wind speed while the electrical load remains unchanged. The average wind speed is about 5.5 m/s and the wind speed has an important turbulence component. Figure 14 illustrates results controlled system behaviour.

The speed reference and the anticipative control component were generated according to the wind speed value.

In Figure 14a) one observes the evolution of the wind speed which acts on the turbine rotor. Figure 14b) shows good tracking performances of the speed control loop, Figure 14c) – the mechanical and electrical power evolutions, Figure 14d) – the control input evolution (chopper duty cycle), Figure 14e) – the power coefficient deviation from its maximal value, Figure 14f) – the tip speed ratio evolution, λ, around the optimal value (λ_{opt}=7), Figure 14g) – the DC load current evolution and finally Figure 14.h) shows the trajectory of the operation point around ORC.

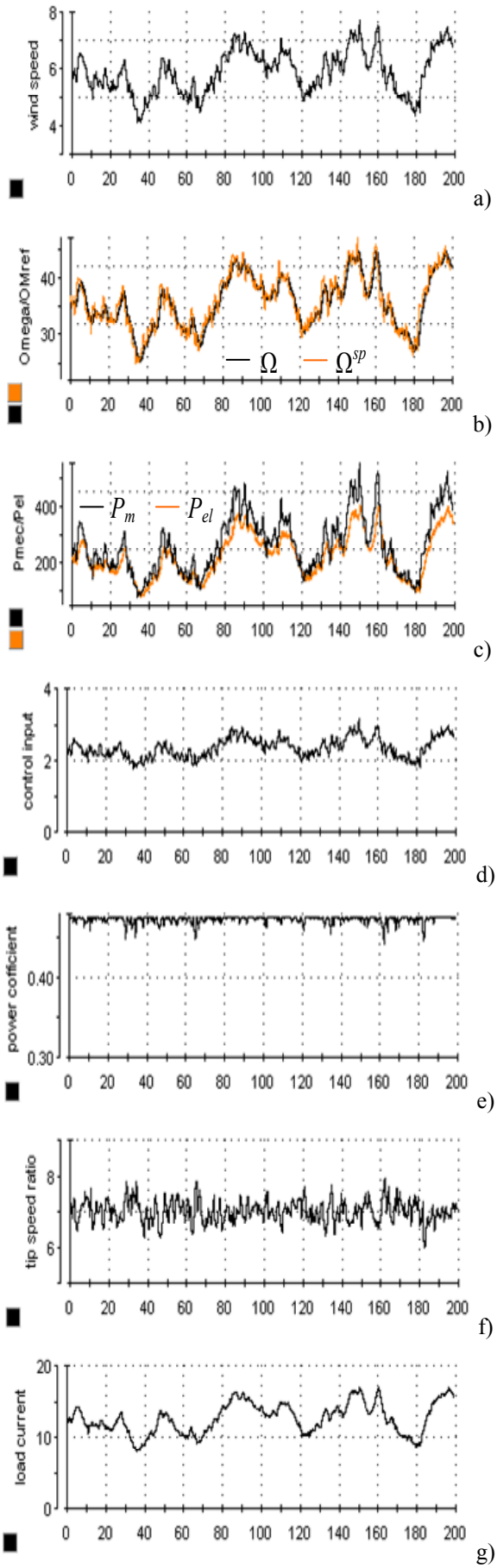

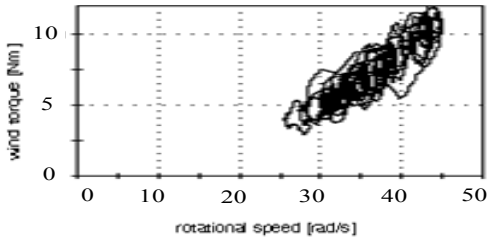

Fig. 14. Screenshot from ControlDesk® interface for speed control loop: anticipative control case

5. CONCLUDING REMARKS

In this paper a new control structure driving the WECS in the partial-load region is introduced. It represents an improvement of the speed control structure ensuring the WECS operation on the ORC. Therefore, this speed control structure can constitute an alternative of the successful power or torque control laws. It introduces less nonlinearities and has the ability of directly managing the turbine rotor speed value in a most uncertain environment generated by the wind speed erratic variations.

The paper highlights the drawbacks of the standard WECS rotational speed structure and proposes some effective solutions for their overcoming. In this context, the closed-loop dynamics are corrected by using an anticipative control structure. This latter result from the analysis of the main perturbation (wind speed) influence on the WECS yielding an important feature of the closed-loop system: the wind speed simultaneously generates the loop reference and the plant disturbance. The reference and disturbance influence the rotational speed in the same sense, causing difficulty in ensuring a good/desired dynamic regime.

The paper provides also a comparative analysis between this new control structure and the classical ones, powered by some advanced controllers as is the case of those resulted from LQ optimal control problems. By assessing both the off-line and experimental results one can ascertain that the anticipative control structure has better dynamic performances, providing better energy efficiency with less control input effort.

The proposed control structure has been experimentally validated, using a complex development system, dedicated to investigation of low-power WECS.

REFERENCES

Arifujjaman, Md. et al. (2008). Energy capture by a small wind-energy conversion system. *Applied Energy*, Vol.85, pp. 41-51.

Bianchi, F. et al. (2006). Wind turbine control systems – Principles, modelling and gain scheduling design. *Springer-Verlag*, London.

Borowy, B. and Salameh, Z.M. (1997). Dynamic Response of a stand-alone wind energy conversion system with battery energy storage to a wind gust. *IEEE Transactions on Energy Conversion*, 12(1), pp. 73-78.

Burton, T. et al. (2001). Wind energy handbook. *John Wiley & Sons*, New-York.

Camblong H. et al. (2006). Experimental evaluation of wind turbines maximum power point tracking controllers. *Energy Conversion and Management* 47(18-19), 2846-2858.

Ceangă, E. et al. (2001). Théorie de la commande des systèmes. *Editura Tehnică*, Bucureşti.

Cutululis, N. A. (2004). Feedback linearization control of wind power systems. *The Annals of "Dunărea de Jos" University of Galati*, Fascicola III, Galați.

Cutululis, N.A. and Ceangă, E. (2004). Robust control of an autonomous wind power. *Control Engineering and Applied Informatics*, 6(4), pp.3-12.

Cutululis, N.A. et al. (2006). Robust multi-model control of an autonomous wind power system. *Wind Energy*, 9(5), pp. 399-419.

De Broe, A.M. et al. (1999). A peak power tracker for small wind turbines in battery charging applications. *IEEE Transactions on Energy Conversion*, 14(4), pp. 1630-1635.

Diop, A.D. et al. (2007). Real-time three-dimensional wind simulation for windmill rig tests. *Renewable Energy*, 32(13), pp. 2268-2290.

Leithead, W.E. et al. (1991). Role and objectives of control for wind turbines. *IEE Proceedings-C,* 138(2), pp.135-148.

Leonhard, W. (2001). Control of electrical drives, 3rd edition. *Springer*, Berlin Heidelberg New-York.

Martinez, J. et al. (2006). Analysis and simulation of a wind-electric battery charging system. *International Journal of Energy Research*, Vol.30, pp. 633-646.

Munteanu, I. et al. (2008). Optimal control of wind energy systems – Towards a global approach. *Springer-Verlag,* London.

Nichita, C. et al. (2002). Large band simulation of the wind speed for real time wind turbine simulators. *IEEE Transactions on Energy Conversion*, 17(4), , pp. 523-529.

Senjiyu, T. et al. (2006). Wind velocity and rotor position sensorless maximum power point tracking control for wind generation system. *Renewable Energy*, Vol.31, pp. 1764-1775.

Tan K. and Islam S. (2004). Optimum control strategies in energy conversion of PMSG wind turbine system without mechanical sensors. *IEEE Transactions on Energy Conversion,* 19(2), 392-399.

Appendix A. Torque coefficient parameters

$a_0 = 0.0061$, $a_1 = -0.0013$, $a_2 = 0.0081$, $a_3 = -9.7477\text{e-}4$, $a_4 = -6.5416\text{e-}5$, $a_5 = 1.3027\text{e-}5$, $a_6 = -4.54\text{e-}7$.

Appendix B. The anticipative controller transfer function

$$H_c(z) = \frac{-0.004057z + 0.00405}{z^2 - 1.9841z + 0.9841}$$